(Received 21 August 2024, Accepted 11 October 2024, Scheduled 22 October 2024)

A Multifunctional Antenna with High Isolation for Interweave and Underlay Operation in Cognitive Radio

Praveen S. Rathore, Ravi Mali, Rajkumar Jatav, and Manoj K. Meshram*

Department of Electronics Engineering, Indian Institute of Technology (BHU), Varanasi 221005, India

ABSTRACT: This paper presents a multifunctional antenna with high isolation for interweave and underlay cognitive radio (CR) applications. The proposed antenna consists of an ultra-wideband (UWB) antenna (ANT1) for sensing and communication in UWB spectrum range and a frequency reconfigurable antenna (ANT2) for communication over frequency ranges from 3 to 3.7 GHz and 3.8 to 5.6 GHz. The proposed antenna is designed on an FR-4 substrate $50 \times 65 \times 1.6\,\text{mm}^3$ with a shared ground plane. A square slot and a rectangular stub is introduced in the ground plane to achieve -10 dB wide impedance bandwidth and good isolation over the frequency range of 1.8 to 12 GHz. An underlay CR operation is attained with a UWB ANT1 with reconfigurable band notch of 2.76 to 3.7 GHz by introducing a U-shaped slot. The interweave operation is obtained by incorporating ANT1 and ANT2 in the same substrate. ANT1 without notch band is used for sensing spectrum, and ANT2 with reconfigurable frequency is used for communication. The proposed antenna attains interweave and underlay operations with inter-port isolation greater than 17 dB all over the proposed UWB and communication band.

1. INTRODUCTION

Federal Communication Commission (FCC) authorized the frequency band of 3.1 to 10.6 GHz for ultra-wideband (UWB) applications [1]. This spectrum is a limited resource, and managing this spectrum effectively is essential to meeting the growing wireless communication needs. Cognitive radio (CR) effectively uses the spectrum and reduces the spectrum congestion. CR systems can adjust and optimize their communication parameters based on user requirements, environment awareness, and real-time spectrum sensing. Two types of users are present in cognitive radio. The primary users can access the spectrum at any moment, while the spectrum is accessible to the secondary users whenever the band is idle. Based on spectrum sharing between primary and secondary users, the CR system is classified as interweave CR and underlay CR [2–4]. Two different types of antennas are needed for interweave CR. The communication is done with a frequency reconfigurable antenna, and for spectrum sensing, a UWB antenna is used.

An antenna with dual ports in the same volume for narrow and wideband operation was reported in [5] for interweave applications. It exhibits one wideband omnidirectional antenna for scanning the spectrum and one narrowband antenna for communication. The interweave CR senses the entire spectrum to identify the underutilized spectrum by using spectrum sensing, and it uses the most appropriate channel from the unused part of the spectrum and permits secondary users to communicate without interfering with primary users. Since two antennas are used in interweave cognitive radio, isolation between ports is required for these antennas.

Underlay CR consists of one antenna, and it allows secondary users to utilize the spectrum concurrently with primary users, as long as their interference level is less than the maximum tolerated. In this case, the secondary users should be restricted transmitted power [6, 7], and a tunable notched wideband antenna is required [8]. The primary and secondary user interference was reduced with the notches in the UWB antenna within its operational frequency range [9].

In the literature, various articles on cognitive radio antennas have been reported [10–19]. A single port CR antenna system was reported in [10, 11]. In [10], a selective frequency reconfigurable antenna was proposed in which the same antenna acted as a sensing and communicating antenna. In [11], the underlay CR with three independently controllable band notches was discussed. In [12], a reconfigurable operating band multiple-input multiple-output (MIMO) antenna within the UWB range was achieved, and a high isolation MIMO antenna with reconfigurable single band elimination was discussed in [13]. A dual port CR antenna system with a wideband sensing antenna and a narrowband communication antenna was reported in [14]. However, the narrowband antenna was limited to the single band of operation. In [15], integrated two-port compact CR with high isolation has been discussed, and the narrowband antenna had two frequency bands of operation. The antenna system reported in [10, 11, 14, 15] is applicable to either underlay CR or the interweave CR. In [16], separate antenna systems have been designed to achieve underlay and interweave CRs. MIMO and CR technologies were combined in [17], and the underlay and interweave CR was achieved using a single antenna system. In [18], an 8-port MIMO antenna has been reported for integrated interweave-underlay operations. However, the frequency of operation for scanning was limited to

* Corresponding author: Manoj Kumar Meshram (mkmeshram.ece@itbhu.ac.in).

sub-6 GHz 5G. In [19], a multi-radio antenna system with integrated UWB MIMO, narrowband MIMO and cognitive radio (CR) was reported. Achieving good isolation while integrating multiple antenna elements on a single substrate is challenging. Various isolation enhancement techniques have been reported in the literature, including defected ground structures, complementary split-ring resonator (CSRR), parasitic stubs, electromagnetic band gap structures (EBG), and extended ground stubs [15, 26, 30–32]. While combining multiple methods can improve isolation, it also increases design complexity. The extended ground stub is less complex and can achieve good isolation [15].

While integrating the two antennas on a single substrate for interweave CR systems, good isolation between antennas is essential. The communication antenna, being reconfigurable antenna, operates across multiple frequency bands, and its higher harmonics are also present. This results in interference between the sensing antenna and communicating antenna.

In an underlay CR system, the secondary users continuously transmit at low power over short distances. A UWB antenna with reconfigurable notches in its operating band is required for this case. Additionally, these notches should be canceled when spectrum sensing is necessary. Therefore, a multifunctional interweave and underlay cognitive radio system with good isolation provides an effective solution for improved spectrum utilization and reduced interference challenges.

This paper proposes a multifunctional antenna for interweave and underlay cognitive radio systems with high isolation. The design includes a UWB antenna (ANT1) for sensing the UWB spectrum, with a reconfigurable single band notch and a frequency reconfigurable antenna (ANT2) for communication purposes. The UWB antenna with a reconfigurable notch band enables underlay CR operation, and when the notch is deactivated, it functions as a sensing antenna. ANT1 and ANT2 together support interweave CR operations. The scanning range covers the entire UWB spectrum, while the notch band helps reduce interference with a major portion of the WiMAX band. The minimum isolation between ANT1 and ANT2 ports is greater than 17 dB in all four operating cases in Table 2. The proposed antenna is designed to achieve interweave and underlay CR operations with good isolation between antenna ports and minimal design complexity. Section 2 discusses the development of ANT1 and ANT2 designs. Antenna performance and findings are presented in Section 3, along with a discussion. This paper concludes in Section 4.

This paper's contributions are as follows:

1. The proposed antenna is beneficial for both interweave CR and underlay CR with a single system and exhibits an ultra-wideband scanning range from 1.86 GHz to 12 GHz, covering a broad spectrum, which is highly suitable for UWB applications.
2. The proposed design employs fewer switching components, reducing the complexity.
3. High port isolation is crucial when two antennas are placed in a CR system. Including an extended stub in the ground plane enhances the antenna's bandwidth (1.86 GHz–12 GHz) and improves the isolation between ANT1 and ANT2 to −17 dB, ensuring better performance and reduced interference.

2. ANTENNA DESIGN

The proposed antenna operates in two states namely state-A and state-B. State-A corresponds to underlay CR. In state-A, ANT1 transmits in UWB with reconfigurable band rejection. It will allow ANT1 to transmit in UWB and minimize the interference with primary users. If the primary user is not able to tolerate the interference level of secondary users, the reconfigurable notch band is required as represented in ANT1. At the same time, state-B corresponds to interweave CR. State-B requires two antennas, ANT1 (without notch band) for constant scanning of the wide spectrum and ANT2 (frequency reconfigurable) for communication. These states are achieved by incorporating a reconfigurable notch band into the UWB antenna (ANT1) and a reconfigurable frequency band in ANT2.

2.1. UWB Antenna (ANT1) Design

In this section, the UWB antenna (ANT1) is designed and discussed. Our main aim is to design an antenna that can sense and communicate within the UWB frequency range. The UWB antenna (ANT1) is designed with the proper substrate, patch, and ground plane selections. The substrate is FR-4 epoxy with relative permittivity $\varepsilon_r = 4.4$, dielectric loss tangent ($\tan\delta$) of 0.02, and thickness of 1.6 mm. The frequency reconfigurable antenna (ANT2) is also incorporated within the same substrate. The circular patch antenna (ANT1) with radius $R_1 = 12$ mm and partial ground plane is similar to [20], except for extended ground plane. The design steps for the UWB antenna (ANT1) from Step 1 to Step 3 are shown in Fig. 1. The electromagnetic (EM) full-wave simulator HFSS version 22.2 [28] is used to simulate the proposed antenna. The ultra-wide bandwidth is achieved by optimizing the partial ground plane, the gap between the circular patch and ground plane, slot on ground plane, and the extended ground plane.

The reflection coefficient of ANT1 is shown in Fig. 2. In Step 1, the circular patch with the ground plane $(L_g \times W_g)$ mm^2 achieves the lower cutoff frequency of 2.24 GHz. The partial ground plane helps to achieve the wide bandwidth of (2.24–6.34 GHz). However, UWB (3.1–10.6 GHz) is not achieved.

In Step 2, the impedance bandwidth is improved with a square slot $(L_1 \times W_1)$ mm^2 in the partial ground plane to achieve a bandwidth of 9.77 GHz (2.23–12 GHz). In Step 3, the ground plane is extended with a rectangular stub $(L_{g1} \times W_{g1})$ mm^2, further enhancing the bandwidth to 10.14 GHz (1.86–12 GHz). Moreover the extended ground plane also improves the isolation between ANT1 and ANT2.

2.1.1. UWB Antenna (ANT1) with a Reconfigurable Single Band Notch for Underlay CR

The UWB antenna (ANT1) allows the secondary user to transmit over UWB. The interferences with primary users can be minimized by introducing the notch band at specific frequencies in communicating with a wideband antenna. To achieve

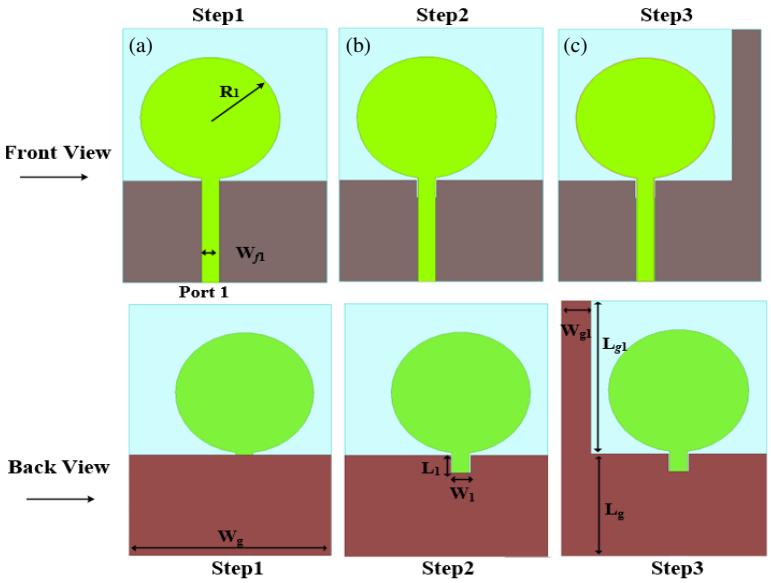

FIGURE 1. Evolution of UWB antenna (ANT1). (a) Step 1, (b) Step 2, (c) Step 3.

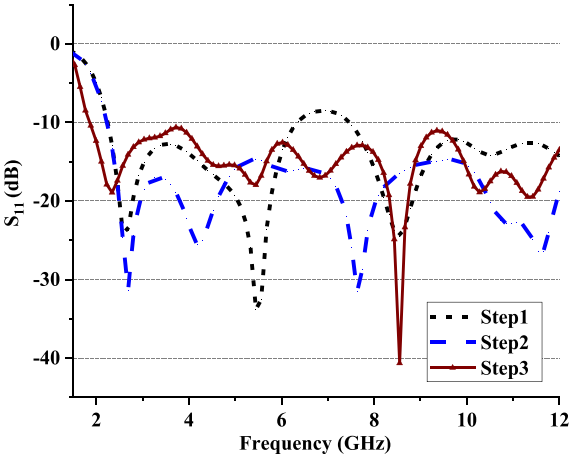

FIGURE 2. Simulated S_{11} of the ANT1.

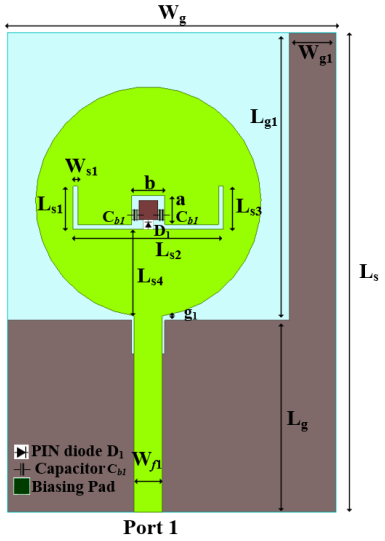

FIGURE 3. UWB antenna with reconfigurable single notch band (ANT1).

the reconfigurability of the notch bands, switching circuits with a PIN diode are used. Fig. 3 depicts the reconfigurable single notch band antenna (ANT1).

In the monopole antenna, a U-shaped slot achieves the notch band for the Wi-MAX band. The resonant band notch frequency is given by [21].

$$f_{\text{notch}} = \frac{c}{2L_{\text{slot}} \times \sqrt{(\varepsilon_{reff})}} \tag{1}$$

$$\varepsilon_{reff} = \frac{\varepsilon_r + 1}{2} \tag{2}$$

where c is speed of light in vacuum; ε_r is the dielectric constant of the substrate; ε_{reff} is the effective dielectric constant calculated by Equation (2); L_{slot} = length of U-shaped slot and f_{notch} = resonant frequency correspond to 3.5 GHz for which L_{slot} is approximately one-half wavelength of the desired notched frequency at 3.5 GHz [22]. The parametric analysis of slot length L_{slot} is shown in Fig. 4. It is observed that the notch band center frequency decreases from 3.7 GHz to 3.3 GHz, with the increase of the slot length from 24.5 mm to 26.5 mm. The simulated voltage standing wave ratio (VSWR) of ANT1 for different L_{slot} is depicted in Fig. 4.

The slot length (L_{slot}) controls the desired notched band frequency. The effect of slot width (w_{s1}) variation on VSWR (keeping the L_{slot} constant at 25.5 mm) is depicted in Fig. 5.

It is observed from Fig. 5 that slot width (w_{s1}) has an insignificant effect on the notch band. However, it is slightly shifted towards lower frequencies with an increase in the width of the slot. Hence, slot length L_{slot} and slot width (w_{s1}) are the parameters that help to design the desired notch band. The shape parameters of the U-shaped slot are analyzed and selected as $L_{\text{slot}} = 25.5$ mm and $w_{s1} = 0.5$ mm.

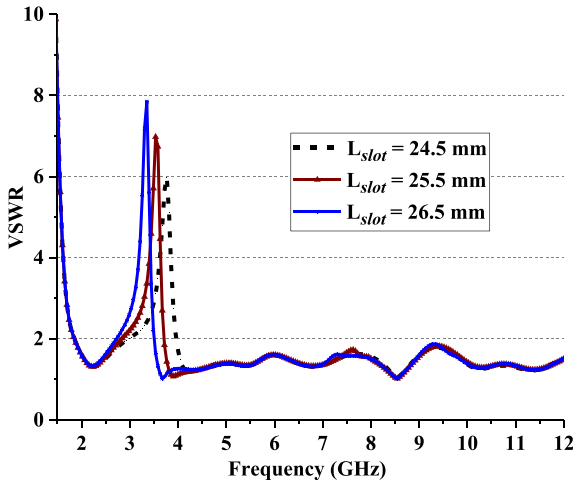

FIGURE 4. VSWR for different values of L_{slot}.

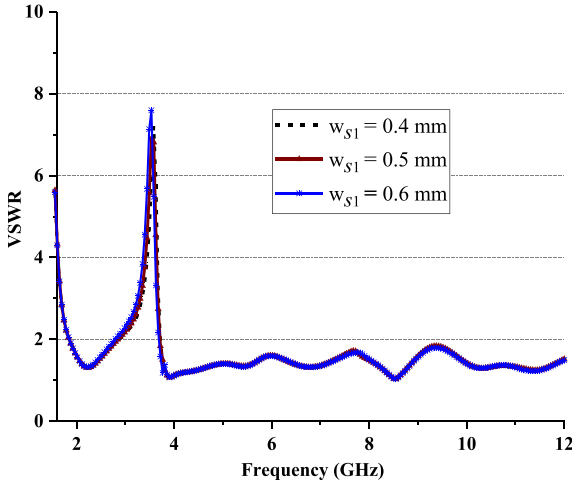

FIGURE 5. VSWR for different values of w_{s1}.

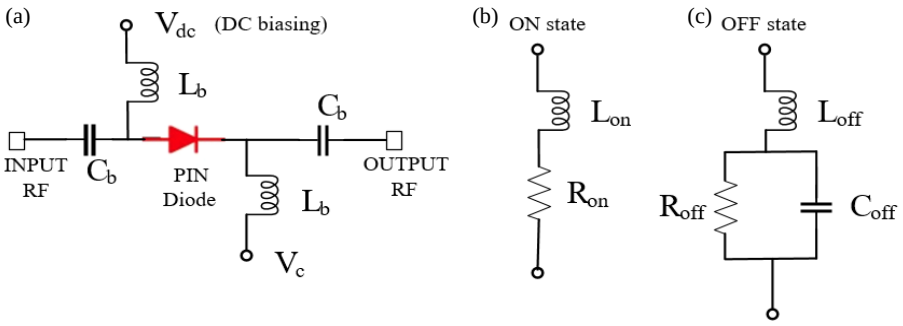

FIGURE 6. (a) Equivalent circuit of RF switch with biasing voltage, blocking capacitor and RF chokes, and PIN diode equivalent circuit, (b) ON state (forward bias), (c) OFF state (reverse bias).

In interweave CR, ANT1 is utilized for scanning the entire UWB without notch band characteristics and a frequency reconfigurable antenna for communication. However, in the case of underlay CR, the UWB antenna (ANT1) should transmit over a UWB with a switchable notch frequency. Therefore, the UWB antenna with or without a notch band is required to utilize the overall UWB efficiently. To attain the notch band for the Wi-MAX band, a PIN diode (SMP-1321-079LF) D_1 is used in a U-shaped slot as depicted in Fig. 6. The PIN diode D_1 can operate in a forward bias (ON state) or reverse bias (OFF state). The PIN diode is modeled as lumped RLC with distinct boundaries in ON and OFF states in fullwave simulations [15]. D_1 in ON state is modeled as a resistor ($R_{\text{on}} = 1.05\,\Omega$) in series with an inductor ($L_{\text{on}} = 0.7\,\text{nH}$). D_1 in the OFF state is modeled as a capacitor ($C_{\text{off}} = 0.18\,\text{pF}$) in series with an inductor ($L_{\text{off}} = 0.7\,\text{nH}$) [23]. The two capacitors (C_{b1}) of values 10 pF are connected to the biasing pad and a radiator to block the DC. With the external DC biasing, when the PIN diode D_1 is ON, the current can flow through the radiator patch. Therefore, UWB is achieved. However, when the PIN diode D_1 is OFF, the slot length produces a band notch at 3.5 GHz (2.8–3.7 GHz) because the surface current is mostly confined in a U-shaped slot. In fabrication, the diode D_1 biasing is done by external DC voltage. Diode D_1 in the ON state exhibits 0.85 Volt across it, and the forward current is 10 mA [23]. Radio frequency (RF) chokes (L_b) block the RF current towards DC biasing voltage. The equivalent circuit of the RF switch with biasing voltage is depicted in Fig. 6. The VSWR and S_{11} of UWB antenna (ANT1) with a PIN diode D_1 in the ON state and OFF state are given in Figs. 7(a) and (b).

It is evident from Fig. 7 that the notch band is achieved for the Wi-MAX band when PIN diode D_1 is in the OFF state. However, UWB is achieved while PIN diode D_1 is in the ON state.

2.2. Frequency Reconfigurable Antenna (ANT2) Design

The frequency reconfigurable antenna (ANT2) is shown in Fig. 8. It is printed on the same substrate material with relative permittivity $\varepsilon_r = 4.4$, dielectric loss tangent ($\tan\delta$) of 0.02, and thickness of 1.6 mm. ANT2 is excited using a microstrip feed line width (W_{f2}) of 3 mm to match a 50 Ω impedance. The partial ground plane length is L_g (mm), and width is W_{g2} (mm). The partial ground plane is considered to obtain a nearly omnidirectional pattern [24].

PIN diode D_2 is modeled similarly to the diode D_1 in simulation. The capacitor C_{b2} (100 pF) blocks the DC to Port 2. RF chokes L_b (100 nH) obstruct the RF towards external DC biasing voltage. By adjusting the length of ANT2, PIN diode (D_2) is utilized to accomplish frequency reconfigurability. PIN diode (D_2) has two states: ON state and OFF state. ANT2 is

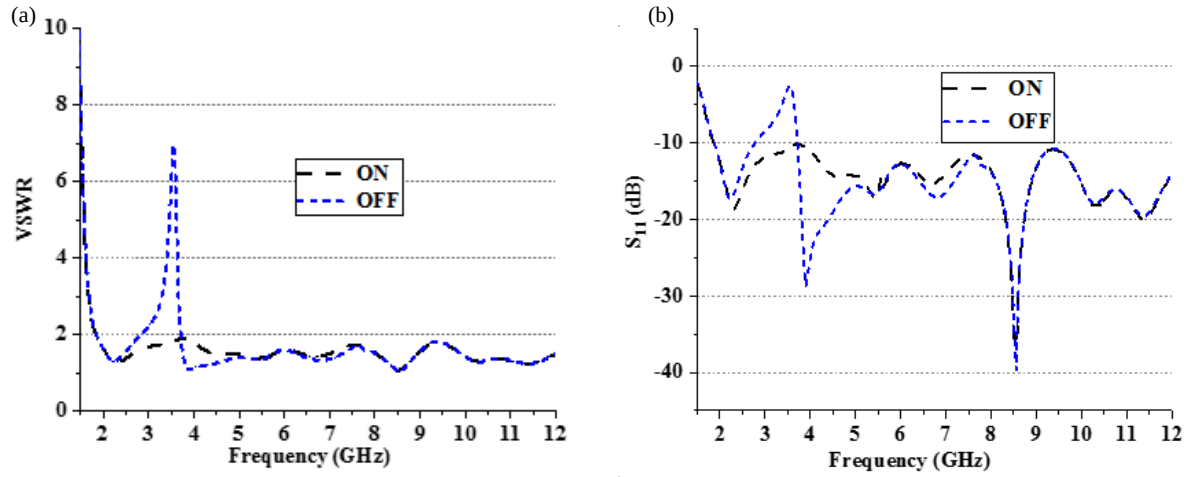

FIGURE 7. (a) VSWR of ANT1 when D_1 ON and OFF, and (b) S-parameter (S_{11}) of UWB antenna (ANT1) with PIN diode D_1 in ON state and OFF state.

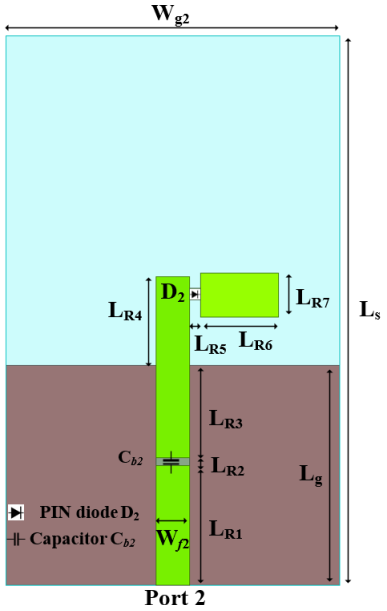

FIGURE 8. Frequency reconfigurable antenna (ANT2).

designed with a size of $(L_s \times W_{g2})$ mm^2 and length L_{R4} to generate the resonance in a higher frequency band at 5 GHz with diode D_2 in OFF state. ANT2 covers the frequency of WLAN (5/5.2/5.8 GHz) and ISM bands (5.2 GHz/5.8 GHz). When diode D_2 is in ON state, it resonates at 3.4 GHz due to an increase in the antenna length. To generate lower frequency band resonance, the length of ANT2 is extended with a rectangular shape stub of size ($L_{R6} \times L_{R7}$). The operating lower band of ANT2 is the same as the frequency band notched from the UWB. Hence, ANT1 with notch band and ANT2 as secondary user will provide this configuration to operate underlay CR.

The ANT2 performance with extended ground plane is also studied. The extended ground plane is the total ground plane of ANT1 and ANT2. Figs. 9(a) and (b) present ANT2 performance with different ground planes in diode D_2, ON and OFF states. From Fig. 9(b), it is observed that the extended ground plane has a slight effect on impedance bandwidth and the resonant frequency of ANT2. The resonant frequency shifted slightly lower in both the cases for diode D_2 ON and OFF states with the resonant frequency of 3.33 GHz and 4.7 GHz, respectively [14, 25–27].

2.3. Design of Proposed Multifunctional Antenna for Underlay CR and Interweave CR

The multifunctional antenna in Fig. 10 consists of an ultra-wideband antenna (ANT1) with a reconfigurable single band notch and an ANT2 with frequency reconfigurability. Both antennas are adjacent on one substrate board to make it compact. The resultant multifunctional antenna does not use any additional decoupling network/elements. Two PIN diodes D_1 and D_2 operate in ON and OFF states, and its four combination states are listed in Table 2. The S-parameters for all four states are depicted in Figs. 11(a), (b), (c), and (d). It is evident that more than 17 dB isolation between antenna elements is achieved across the entire UWB frequency range in all four states. ANT1 covers the frequency band of 1.87 to 12 GHz in each of these states, and when D_1 is in the OFF state, the notch band of 2.76 to 3.7 GHz is achieved. ANT2 covers the frequency band of 3.02 to 3.7 GHz and 3.83 to 5.65 GHz for D_2, ON and OFF states, respectively.

The optimized antenna design parameters are listed in Table 1.

Table 2 depicts the conditions of PIN diode states. Here State_1, State_2 is utilized for underlay CR and State_3, State_4 works for interweave CR.

3. RESULTS AND DISCUSSION

The antenna prototype shown in Fig. 12 is made with an MITS-eleven lab prototyping machine. A biasing pad is used to apply DC biasing voltage for the biasing of PIN diode D_1. Measurement and validation of the simulated findings from the proposed antenna are done by VNA Master MS2038C.

TABLE 1. Design parameter of the proposed antenna.

Design parameter	Value (mm)	Design parameter	Value (mm)	Design parameter	Value (mm)	Design parameter	Value (mm)
L_s	50	a	3	W_{f1}	3	L_{R3}	8.4
L_g	20	b	3.5	W_g	35	L_{R4}	8.25
L_{g1}	30	g_1	0.47	W_{g1}	5	L_{R5}	1
L_{s1}	4.5	L_1	3.5	W_{g2}	30	L_{R6}	7
L_{s2}	16	W_1	3.5	W_{f2}	3	L_{R7}	4
L_{s3}	4.5	W_s	65	L_{R1}	10.9		
L_{s4}	9	W_{s1}	0.5	L_{R2}	0.7		

TABLE 2. PIN diode states, ANT1 with notch band and ANT2 band of operations.

State	PIN Diode (D_1)	PIN Diode (D_2)	Frequency Band ANT1 (GHz)	Notch band in ANT1 (GHz)	Frequency Band ANT2 (GHz)
State_1	OFF	OFF	1.86–12	2.76–3.72	3.83–5.65
State_2	OFF	ON	1.87–12	2.76–3.79	3.02–3.70
State_3	ON	OFF	1.8–12	-	3.82–5.66
State_4	ON	ON	1.8–12	-	3–3.71

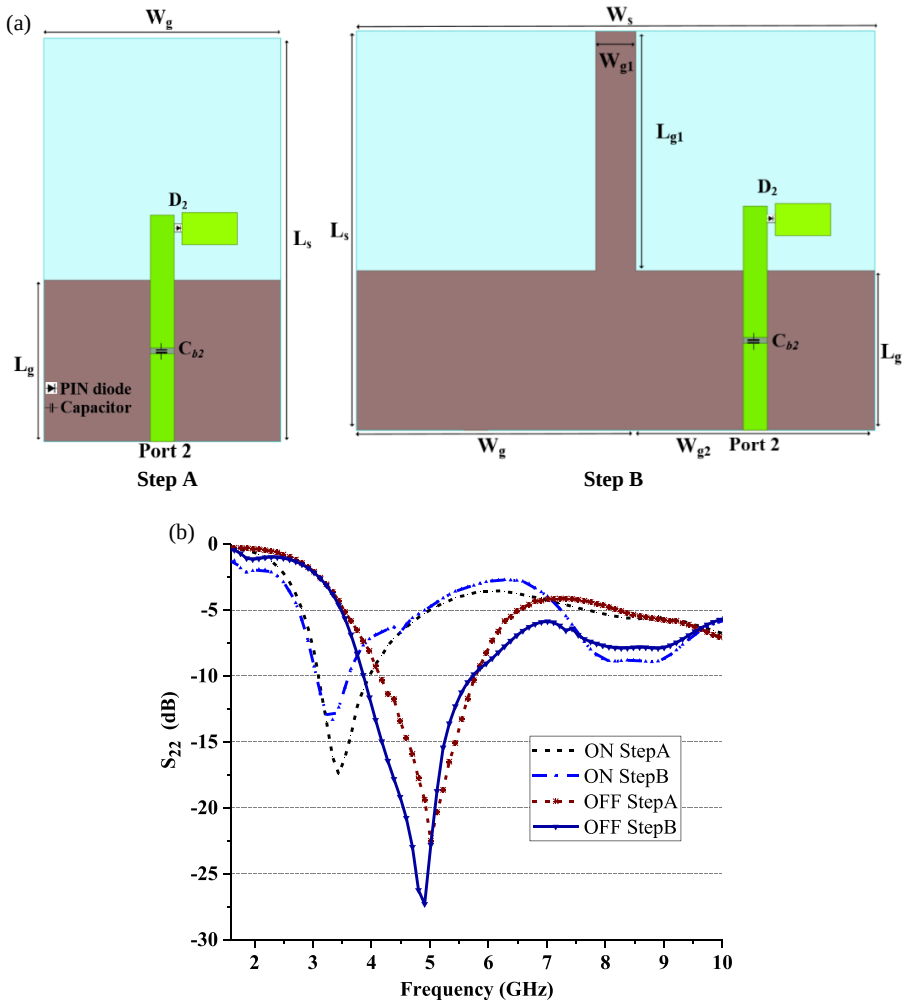

FIGURE 9. (a) ANT2 with different ground planes: Step A and Step B, (b) S_{22} (dB) with different ground planes in diode D_2 ON and OFF states.

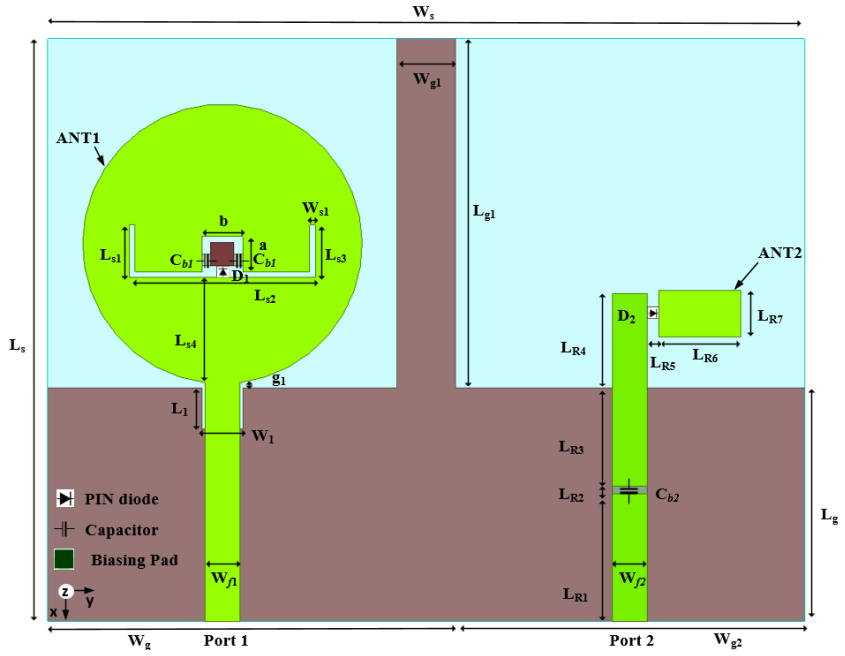

FIGURE 10. Proposed antenna schematic diagram.

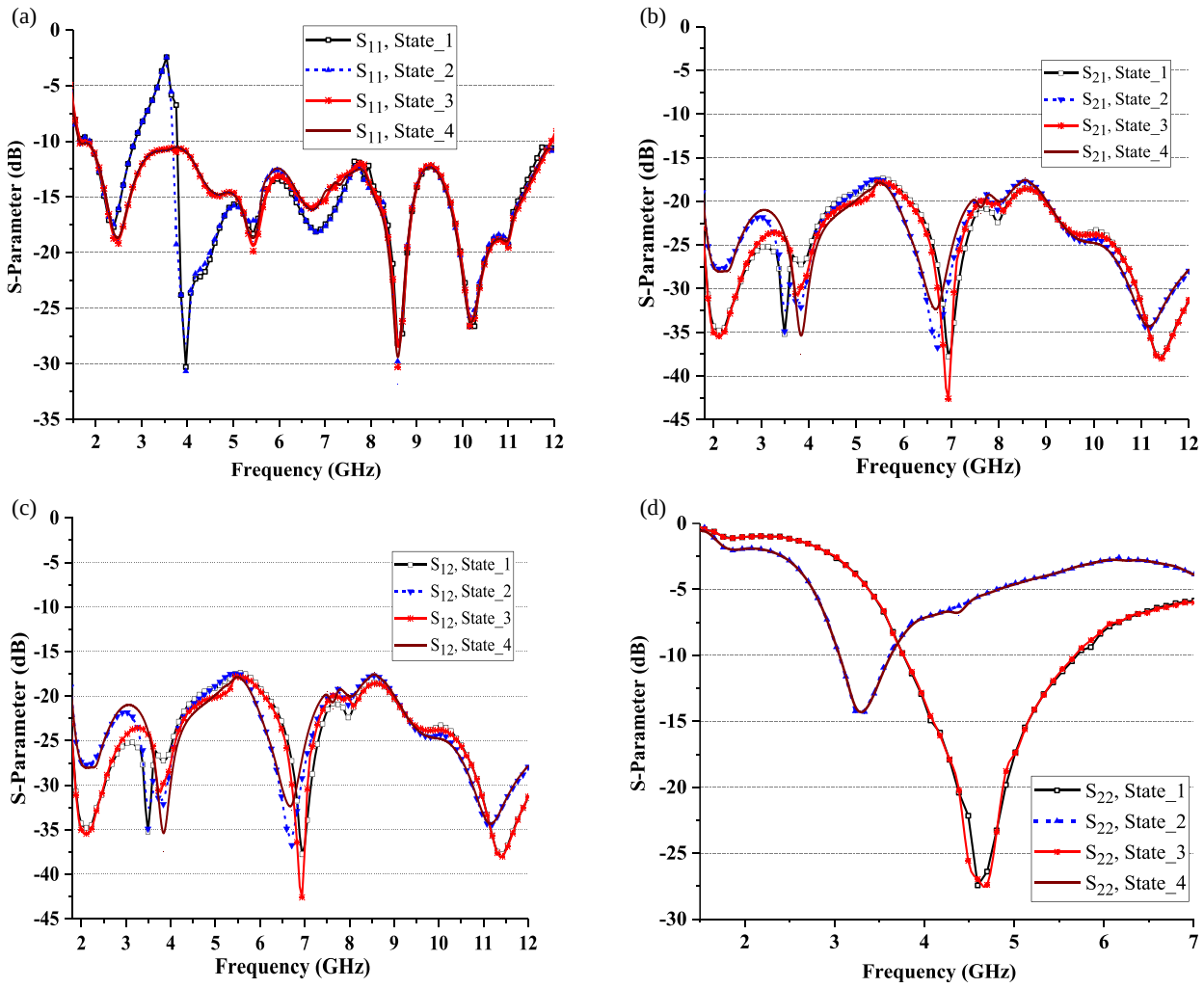

FIGURE 11. Simulated S-parameters for all four states: (a) S_{11}, (b) S_{21}, (c) S_{12}, (d) S_{22}.

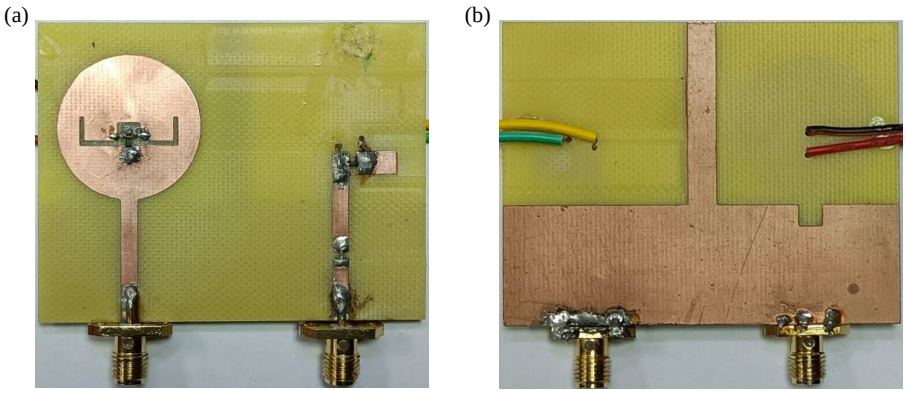

FIGURE 12. Fabricated prototype of proposed antenna. (a) Top view. (b) Bottom view.

3.1. S-Parameters Measurement

The simulated and measured reflection coefficients (S_{11}, S_{22}) and coupling coefficients (S_{12}, S_{21}) for ANT1 and ANT2 with four states are shown in Figs. 13(a), (b), (c), and (d). While S_{11} is measured, Port 1 (ANT1) is excited, and Port 2 (ANT2) is matched terminated. The measured impedance bandwidth for ANT1 in the D_1 OFF state is 10.1 GHz (1.9–12 GHz) with a notch band of 2.7 GHz to 3.7 GHz. ANT1 has a measured bandwidth of 10.2 GHz (1.8–12 GHz) without any notch band in diode D_1 ON state. While S_{22} is measured, Port 2 is excited, and Port 1 is matched terminated. The measured impedance bandwidth for ANT2 is 3.03–4.29 GHz and 3.73–5.55 GHz for D_2 ON and OFF states, respectively, and it is shown in Figs. 13(a) and (b). The measured isolations S_{12} and S_{21} are less than -17 dB in most of the operating frequencies as depicted in Figs. 13(c) and (d). The measured -10 dB reflection and transmission coefficient performance of the prototype have good agreements with the simulated ones. Minor inconsistency is observed due to fabrication errors.

3.2. Radiation Patterns and Gain

The radiation patterns and gain measurements are carried out. The performance characteristics of the designed antenna are verified by the fabricated prototype, as shown in Fig. 14. A broadband horn antenna (1–18 GHz) is employed at the transmitting end, and at the receiving end, the proposed antenna is in far-field distance. When Port 1 (ANT1) is excited, and Port 2 (ANT2) is matched terminated, the radiation patterns are measured at 2.4 GHz, 3.9 GHz, and 6.8 GHz for both the (D_1) ON and OFF cases. Similarly, the radiation patterns of ANT2 are measured at frequencies 3.3 GHz (D_2 is ON state) and 4.7 GHz (D_2 OFF state) while keeping Port 2 excited and Port 1 matched terminated with 50 Ω.

Figures 15(a), (b), (c), (d) depict the measured and simulated 2D radiation patterns of ANT1 at frequencies 2.4, 3.9, and 6.8 GHz in xz and yz-planes, with acceptable agreement. It is noted that in E-plane (xz) at lower frequencies, the radiation pattern is directional; however, at higher frequencies, the antenna exhibits a slightly skewed radiation pattern because of the current distribution in the extended stub [15, 25]. Same as the H-plane (yz) radiation pattern is also slightly directional at frequencies 2.4 GHz, 3.9 GHz, and 6.8 GHz. Cross-polarization is observed to be more than 12 dB in all four cases.

The measured radiation patterns of ANT2 in E- and H-plane are shown in Figs. 16(a) and 16(b).

The E-plane (xz) and H-plane (yz) radiation patterns are directional in diode D_2 ON and OFF cases, caused by the extended stub. The pattern asymmetry is due to the extended stub. The cross-polarization is more than 12 dB in diode D_2 ON and OFF cases.

ANT1 has a positive gain across the UWB frequency range (1.8–12 GHz) except the notched frequency band. The U-shaped slot gives the desired band notch characteristics, and ANT1 has a very good impedance matching at other UWB frequencies. ANT2 exhibits a positive gain throughout the communication frequency range when diode D_2 is in both ON and OFF states. Figs. 17(a) and (b) show a good agreement between measured and simulated realized gains for ANT1 and ANT2.

3.3. Surface Current Distribution

The inter-port isolation can be explained by the surface current distribution [15]. The surface current distributions on ANT1 and ANT2 are plotted for four different states of PIN diodes D_1 and D_2 as depicted in Figs. 18(a), (b), (c), and (d). In State_1, Fig. 18(a), diode D_1 and D_2 are in OFF states. While Port 1 is excited and Port 2 terminated with 50 Ω matched impedance, the current is plotted at a frequency of 3.54 GHz. The surface current is mainly confined to the U-shaped slot, which verifies the band notch response. Similarly, when Port 2 is excited and Port 1 terminated with 50 Ω matched impedance, the surface current distribution is plotted for ANT2 at the resonant frequency of 4.59 GHz. In State_2, Fig. 18(b), PIN diode D_1 is in OFF state, and D_2 is in ON state. A similar notch band can be observed in ANT1, but ANT2 resonates at a low frequency of 3.3 GHz due to increased path length. In State_3 and State_4, diode D_1 is ON in both cases, and diode D_2 is OFF and ON, respectively. When Port 1 is excited, ANT1 operates in the UWB frequency range without any notch band. The surface current distribution in Figs. 18(c) and (d) shows that the current is not confined near the U-shaped slot, and it confirms the UWB radiation of ANT1, whereas ANT2 operates in State_3 and State_4 at 4.7 GHz and 3.3 GHz, respectively. In addition, the isolation

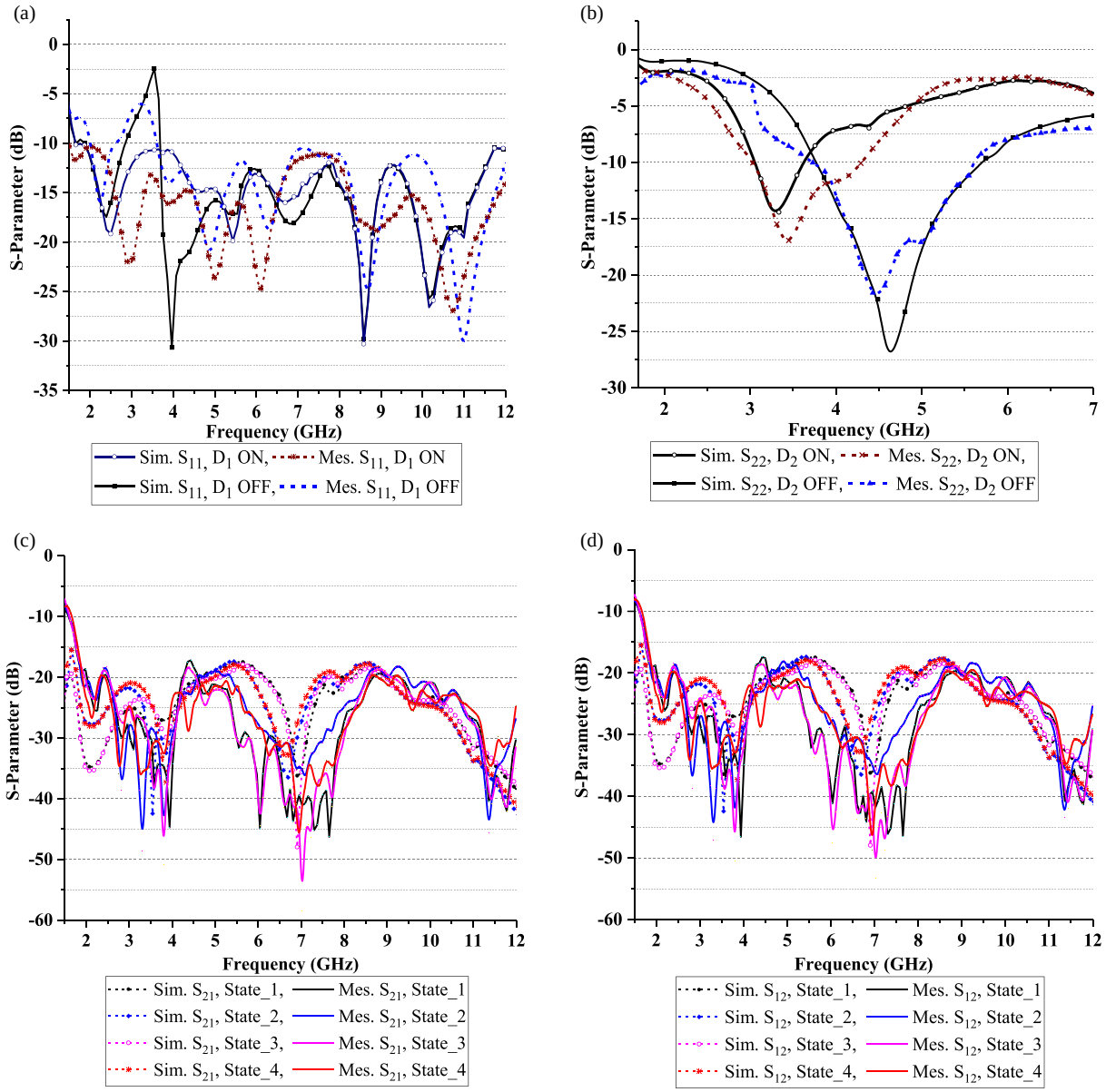

FIGURE 13. Simulated and measured S-parameters of proposed antenna. (a) S_{11}, (b) S_{22}, (c) S_{21}, (d) S_{12}.

FIGURE 14. Fabricated prototype antenna in an anechoic chamber.

between antennas can be observed because low surface current is found near Port 1 and Port 2 when Port 2 and Port 1 are excited, respectively.

3.4. Diversity Performances

To analyze the inter-port isolation, the diversity performance of the proposed antenna is calculated. The envelope correlation coefficient (ECC) and diversity gain (DG) by using S-parameters of the proposed antenna are computed and depicted in Figs. 19(a) and (b). The ECC and DG are calculated by [15, 29].

$$\mathrm{ECC} = \frac{\left|S_{11}^{*}S_{12} + S_{21}^{*}S_{22}\right|^{2}}{\left(1-\left(\left|S_{11}\right|^{2}+\left|S_{21}\right|^{2}\right)\right)\left(1-\left(\left|S_{22}\right|^{2}+\left|S_{12}\right|^{2}\right)\right)} \quad (3)$$

$$\mathrm{DG} = 10\sqrt{1-\left|\mathrm{ECC}\right|^{2}} \quad (4)$$

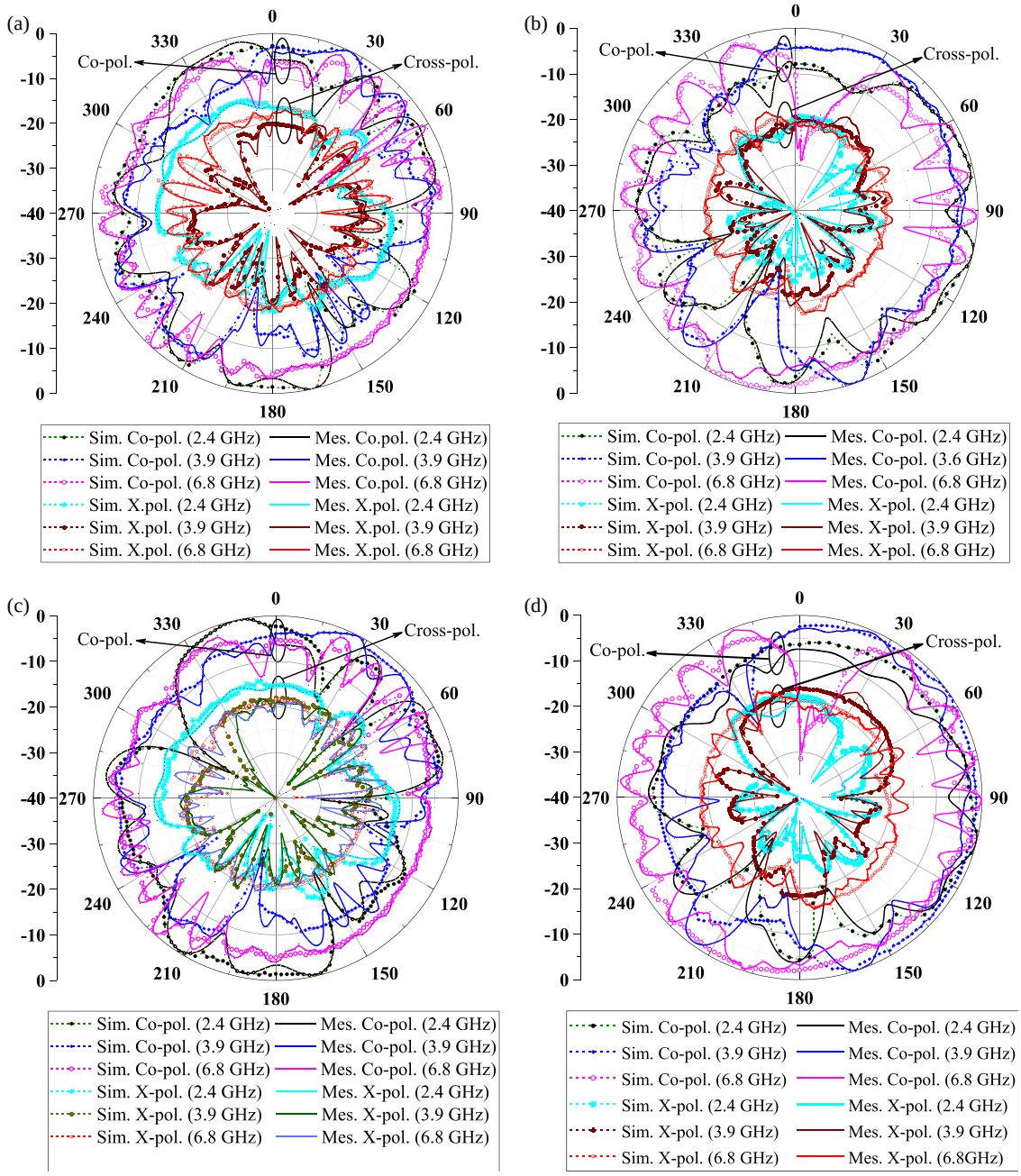

FIGURE 15. Radiation patterns for ANT1. (a) Radiation pattern for ANT1, E-plane (D_1 ON). (b) Radiation pattern for ANT1, H-plane (D_1 ON). (c) Radiation pattern for ANT1, E-plane (D_1 OFF). (d) Radiation pattern for ANT1, H-plane (D_1 OFF).

A lower ECC (< 0.5) and (DG $= 10$) is required for the antenna to perform better in terms of diversity. For all four states, State_1, State_2, State_3, and State_4, the measured ECC is less than 0.22 across the UWB. The measured DG is above 9.8 across the UWB. It shows a good diversity performance of the proposed antenna.

Channel capacity loss (CCL) represents the maximum achievable transmission rate at which a signal can be efficiently transferred without experiencing significant loss, and it should be less than 0.4 bits/s/Hz. The CCL affects the diversity performance of the proposed antenna, and it is calculated by [30]

$$\text{CCL (dB)} = -\log_2\left[\det(\varphi^R)\right] \tag{5}$$

where (φ^R) is a 2×2 S-parameter correlation matrix and $\varphi_{ii} = 1 - |S_{ii}|^2 - |S_{ij}|^2$, and

$$\varphi_{ij} = -\left(S_{ii}^* \times S_{ij} + S_{ji}^* \times S_{jj}\right)$$

The measured and simulated CCLs, shown in Fig. 19(c), exhibits values less than one bits/s/Hz within the operating range of ANT2. The observed discrepancy is attributed to the difference between the simulated and measured S-parameters.

When two port antenna elements work simultaneously, the system performance is evaluated using the total active reflec-

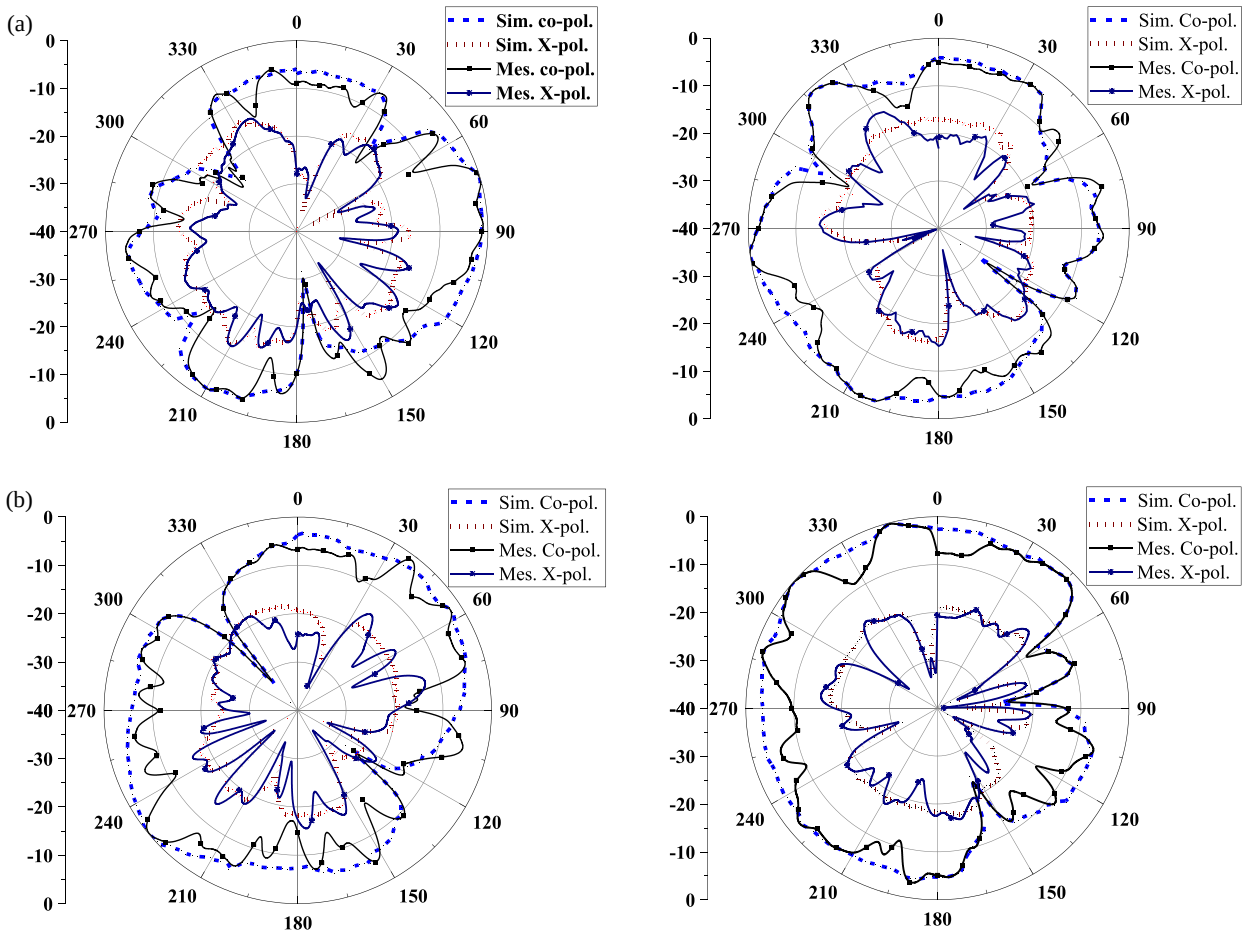

FIGURE 16. Simulated and measured normalized radiation patterns for ANT2. (a) E- and H-plane at 3.3 GHz, D_2 ON. (b) E- and H-plane at 4.7 GHz, D_2 OFF.

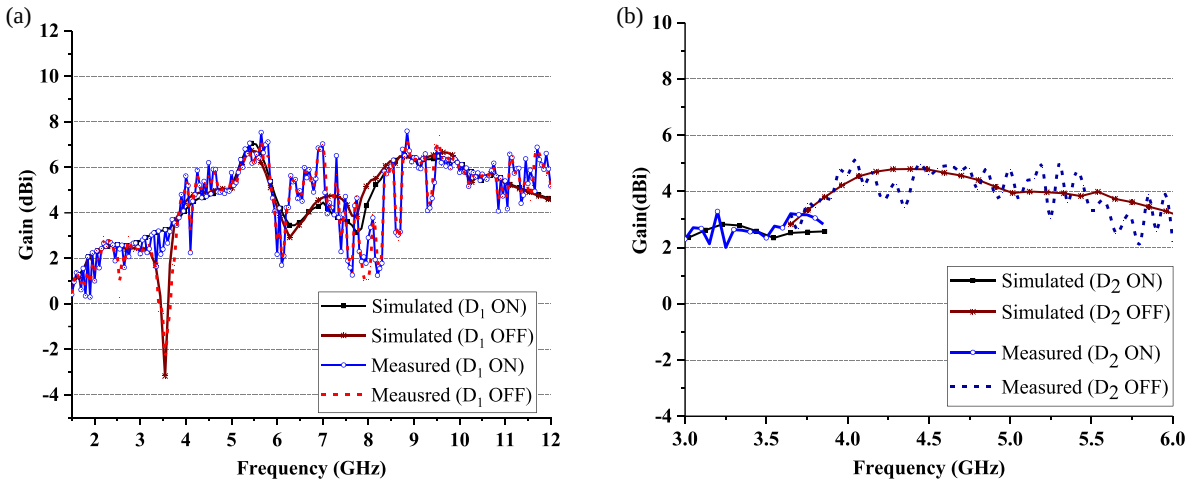

FIGURE 17. Realized gain. (a) ANT1, (b) ANT2.

tion coefficient (TARC). TARC is defined as the square root of the ratio of total reflected power and total incident power. Ideally, the TARC should be (< 0 dB). For two port radiating antenna system, TARC is given by Equation (6) [30].

$$\sqrt{\frac{(S_{ii}+S_{ij})^2+(S_{jj}+S_{ji})^2}{2}} \tag{6}$$

The simulated and measured TARCs shown in Fig. 19(d) of the designed antenna are less than -10 dB in the operating band of ANT2 except for the notched band.

The mean effective gain (MEG) can be calculated by using propagation statistics and radiation patterns. In the fading environment, MEG for the proposed antenna is extracted by the

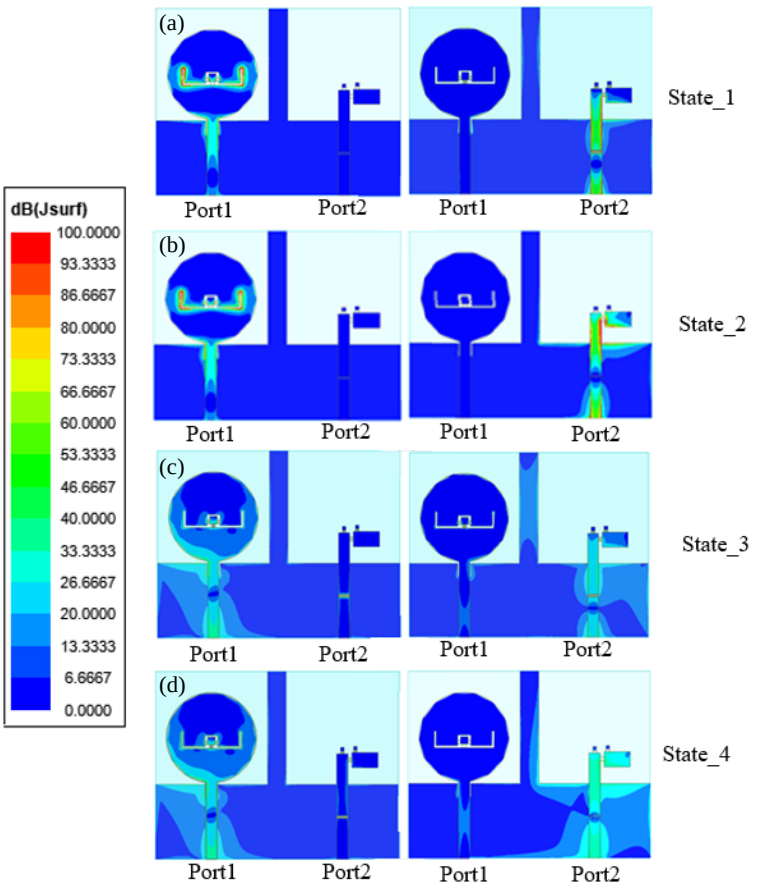

FIGURE 18. Surface current distribution in four different states: (a) State_1 (D_1 OFF, D_2 OFF), (b) State_2 (D_1 OFF, D_2 ON), (c) State_3 (D_1 ON, D_2 OFF), (d) State_4 (D_1 ON, D_2 ON).

TABLE 3. Comparison study with reported work.

Ref.	Type of CR	Size (in terms of $^*\lambda_g$)	UWB antenna range (GHz)	Narrow band antenna range (GHz)	Notch band (GHz)	Isolation (dB)	Ports	Switch (PIN diode/ Varactor diode)
[10]	Underlay	$0.97\lambda_g \times 0.72\lambda_g \times 0.02\lambda_g$	2.63–3.7	2.63–3.7	2.63–3.7 (4 tuning bands)	-	1	12 PIN diodes
[11]	Underlay and Overlay	$0.5\lambda_g \times 0.38\lambda_g \times 0.01\lambda_g$	2–10	2–10	3 band notches at 2.4, 3.5, 5.5	-	1	4 switches
[14]	Interweave	$0.54\lambda_g \times 0.54\lambda_g \times 0.01\lambda_g$	2–11	4.63–6.42	-	< -25 dB	2	-
[15]	Interweave	$0.36\lambda_g \times 0.53\lambda_g \times 0.02\lambda_g$	2.7–10	4.3–5.5 5.1–6.8	-	< -21 dB	2	1 PIN diode
[17]	Interweave and Underlay	$1.64\lambda_g \times 1.36\lambda_g \times 0.02\lambda_g$	2.5–4.2	2.8–3.65	2.15–3.3	< -15 dB	4	20 PIN diodes 4 Varactor diodes
[18]	Interweave and Underlay	$1.5\lambda_g \times 0.93\lambda_g \times 0.02\lambda_g$	2.5–4.2	2.5–4.2	3.1–3.85	< -18 dB	8	12 PIN diodes 16 Varactor diodes
This work	Interweave and Underlay	$0.49\lambda_g \times 0.64\lambda_g \times 0.01\lambda_g$	1.8–12	3–3.7 3.8–5.6	2.76–3.7	< -17 dB	2	2 PIN diodes

$^*\lambda_g$ is the guided wavelength at the lowest operating frequency.

following equations [31]:

$$\text{MEG}_i = 0.5\left[1 - \sum_{j=1}^{N} \mid S_{ij} \mid^2\right] < -3\,\text{dB} \quad (7)$$

$$\text{MEG}_1 = 0.5\left[1 - \mid S_{11} \mid^2 - \mid S_{12} \mid^2\right] \quad (8)$$

$$\text{MEG}_2 = 0.5\left[1 - \mid S_{21} \mid^2 - \mid S_{22} \mid^2\right] \quad (9)$$

Also

$$\mid \text{MEG}_i - \text{MEG}_j \mid < 3\,\text{dB}. \quad (10)$$

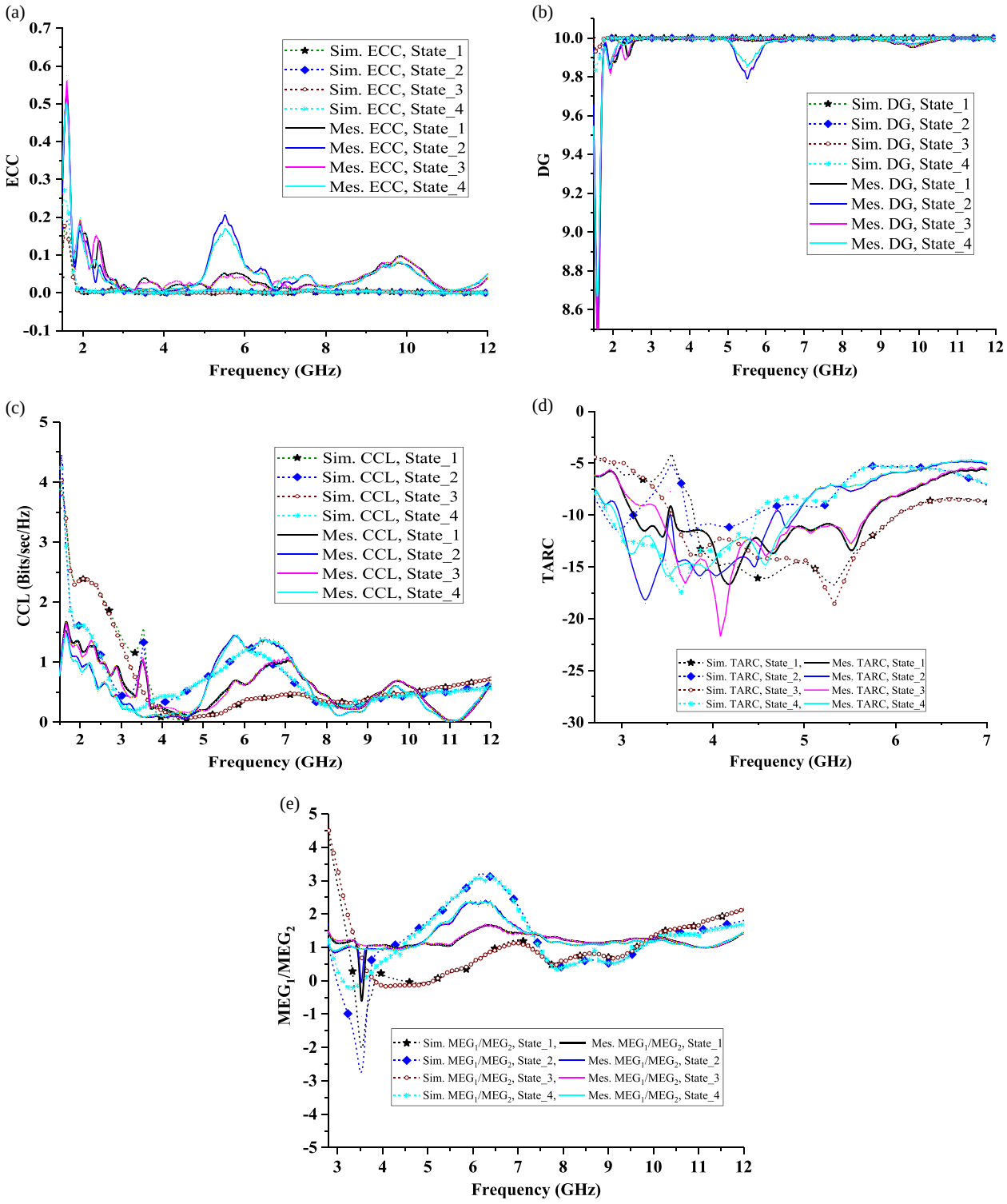

FIGURE 19. Simulated and measured: (a) Envelope correlation coefficient (ECC). (b) Diversity gain (DG). (c) Channel capacity loss (CCL). (d) Total active reflection coefficient (TARC). (e) Mean effective gain (MEG_1/MEG_2).

The value of MEG_i/MEG_j should be close to the unity and within the range of ± 3 dB for satisfactory performance. The ratio of MEG_i/MEG_j is plotted in Fig. 19(e), for the different 4 states of the proposed antenna. It is observed that the measured MEG ratio is in good agreement with the simulated results. The MEG ratio is almost close to 1, excluding the notch band.

Table 3 presents a comparative analysis of the designed antenna with previously reported works based on parameters such as bandwidth, isolation between ports, antenna size, and type. The isolation in [14, 15] is comparatively good, but both works have only interweave operation. The underlay and interweave CRs were achieved in [17, 18] with the frequency of operation

limited up to 4.2 GHz and with an increased number of switching elements. The proposed antenna works in interweave and underlay operations with better than 17 dB isolation between the ports and with only two PIN diodes.

4. CONCLUSION

A multifunctional antenna for interweave and underlay cognitive radios has been investigated. The UWB antenna with a reconfigurable notch band and a frequency reconfigurable antenna provides underlay and interweave operations. The isolation between antenna ports is less than −17 dB. This system provides the sensing range and communicating range of 1.8 GHz to 12 GHz with a reconfigurable notch band of 2.76 GHz to 3.7 GHz and a communicating range of 3 GHz to 5.7 GHz. The proposed antenna also exhibits a good diversity performance and is a suitable candidate for cognitive radio applications.

REFERENCES

[1] Federal Communication Commission (FCC), "Revision of Part 15 of the commission's rules regarding ultra-wideband transmission systems," ET Docket 98-153, FCC 02-48, 2002.

[2] Mitola, J., "Cognitive radio for flexible mobile multimedia communications," in *1999 IEEE International Workshop on Mobile Multimedia Communications (MoMuC'99) (Cat. No.99EX384)*, 3–10, San Diego, CA, USA, 1999.

[3] Goldsmith, A., S. A. Jafar, I. Maric, and S. Srinivasa, "Breaking spectrum gridlock with cognitive radios: An information theoretic perspective," *Proceedings of the IEEE*, Vol. 97, No. 5, 894–914, 2009.

[4] Tawk, Y., M. Bkassiny, G. El-Howayek, S. K. Jayaweera, K. Avery, and C. G. Christodoulou, "Reconfigurable front-end antennas for cognitive radio applications," *IET Microwaves, Antennas & Propagation*, Vol. 5, No. 8, 985–992, 2011.

[5] Ebrahimi, E. and P. S. Hall, "A dual port wide-narrowband antenna for cognitive radio," in *2009 3rd European Conference on Antennas and Propagation*, 809–812, Berlin, Germany, 2009.

[6] Al-Husseini, M., K. Y. Kabalan, A. El-Hajj, and C. G. Christodoulou, "Reconfigurable microstrip antennas for cognitive radio," *Advancement in Microstrip Antennas with Recent Applications*, Vol. 14, 337–362, 2013.

[7] Tawk, Y., J. Costantine, and C. G. Christodoulou, "Cognitive-radio and antenna functionalities: A tutorial," *IEEE Antennas and Propagation Magazine*, Vol. 56, No. 1, 231–243, 2014.

[8] Alam, T., S. R. Thummaluru, and R. K. Chaudhary, "Improved multifunctional MIMO cognitive radio system for integrated interweave-underlay operations," *IEEE Transactions on Microwave Theory and Techniques*, Vol. 70, No. 1, 631–640, 2021.

[9] Tawk, Y., S. K. Jayaweera, C. G. Christodoulou, and J. Costantine, "A comparison between different cognitive radio antenna systems," in *2011 International Symposium on Intelligent Signal Processing and Communications Systems (ISPACS)*, 1–5, Chiang Mai, Thailand, Dec. 2011.

[10] Mansoul, A., F. Ghanem, M. R. Hamid, and M. Trabelsi, "A selective frequency-reconfigurable antenna for cognitive radio applications," *IEEE Antennas and Wireless Propagation Letters*, Vol. 13, 515–518, 2014.

[11] Al-Husseini, M., A. Ramadan, Y. Tawk, C. Christodoulou, K. Kabalan, and A. El-Hajj, "A planar ultrawideband antenna with multiple controllable band notches for UWB cognitive radio applications," in *Proceedings of the 5th European Conference on Antennas and Propagation (EUCAP)*, 375–377, Rome, Italy, 2011.

[12] Durukan, T. and Y. Altuncu, "A compact 4×4 reconfigurable MIMO antenna design with adjustable suppression of certain frequency bands within the UWB frequency range," *AEU — International Journal of Electronics and Communications*, Vol. 170, 154848, 2023.

[13] Saleem, S., S. Kumari, D. Yadav, M. G. Siddiqui, and D. Bhatnagar, "A planar UWB-MIMO antenna with high isolation and reconfigurable single band-elimination characteristics," *AEU — International Journal of Electronics and Communications*, Vol. 170, 154853, 2023.

[14] Naidu, P. R. T., C. Saha, K. V. Krishna, L. A. Shaik, J. Y. Siddiqui, and Y. Antar, "Compact multiple EBG cells loaded UWB-narrowband antenna pair with high isolation for cognitive radio (CR) based MIMO applications," *AEU — International Journal of Electronics and Communications*, Vol. 127, 153420, 2020.

[15] Rathore, P. S., R. Mali, R. Jatav, and M. K. Meshram, "Integrated compact UWB and frequency reconfigurable antenna with high isolation for cognitive radio," *AEU — International Journal of Electronics and Communications*, Vol. 171, 154899, 2023.

[16] Tawk, Y., J. Costantine, and C. G. Christodoulou, "Reconfigurable filtennas and MIMO in cognitive radio applications," *IEEE Transactions on Antennas and Propagation*, Vol. 62, No. 3, 1074–1083, 2014.

[17] Thummaluru, S. R., M. Ameen, and R. K. Chaudhary, "Four-port MIMO cognitive radio system for midband 5G applications," *IEEE Transactions on Antennas and Propagation*, Vol. 67, No. 8, 5634–5645, 2019.

[18] Alam, T., S. R. Thummaluru, and R. K. Chaudhary, "Improved multifunctional MIMO cognitive radio system for integrated interweave-underlay operations," *IEEE Transactions on Microwave Theory and Techniques*, Vol. 70, No. 1, 631–640, 2021.

[19] Kasiselvanathan, M., P. Prabhu, L. Raja, and S. Lebaka, "A multi-radio antenna system for cognitive radio (CR), 5G, WLAN and UWB MIMO applications," *AEU — International Journal of Electronics and Communications*, Vol. 180, 155315, 2024.

[20] Rathore, P. S., R. Mali, R. Jatav, and M. K. Meshram, "A dual-band notched UWB antenna with a slot and a parasitic resonator," in *2023 IEEE Microwaves, Antennas, and Propagation Conference (MAPCON)*, 1–5, Ahmedabad, India, 2023.

[21] Chu, Q.-X. and Y.-Y. Yang, "A compact ultrawideband antenna with 3.4/5.5 GHz dual band-notched characteristics," *IEEE Transactions on Antennas and Propagation*, Vol. 56, No. 12, 3637–3644, 2008.

[22] Wong, K.-L., Y.-W. Chi, C.-M. Su, and F.-S. Chang, "Band-notched ultra-wideband circular-disk monopole antenna with an arc-shaped slot," *Microwave and Optical Technology Letters*, Vol. 45, No. 3, 188–191, 2005.

[23] Skyworks, "Datasheet of (SMP1321-079LF) PIN diodes," [Online], https://www.skyworksinc.com/-/media/skyworks/-documents/products/101-200/smp1321_series_200048z.pdf.

[24] Nella, A., S. K. Vattiprolu, C. Saha, and J. Y. Siddiqui, "A reconfigurable integrated 4-port UWB and NB antenna system for cognitive radio application," *International Journal of RF and Microwave Computer-Aided Engineering*, Vol. 32, No. 3, e22998, 2022.

[25] Liu, L., S. W. Cheung, and T. I. Yuk, "Compact MIMO antenna for portable UWB applications with band-notched characteristic," *IEEE Transactions on Antennas and Propagation*, Vol. 63,

No. 5, 1917–1924, 2015.

[26] Chandel, R., A. K. Gautam, and K. Rambabu, "Tapered fed compact UWB MIMO-diversity antenna with dual band-notched characteristics," *IEEE Transactions on Antennas and Propagation*, Vol. 66, No. 4, 1677–1684, 2018.

[27] Xue, C.-D., X. Y. Zhang, Y. F. Cao, Z. Hou, and C. F. Ding, "MIMO antenna using hybrid electric and magnetic coupling for isolation enhancement," *IEEE Transactions on Antennas and Propagation*, Vol. 65, No. 10, 5162–5170, 2017.

[28] High frequency structure simulator (Ansys HFSS): Ansys Engineering Simulation Software.

[29] Blanch, S., J. Romeu, and I. Corbella, "Exact representation of antenna system diversity performance from input parameter description," *Electronics Letters*, Vol. 39, No. 9, 705–707, 2003.

[30] Saxena, G., P. Jain, and Y. K. Awasthi, "High diversity gain super-wideband single band-notch MIMO antenna for multiple wireless applications," *IET Microwaves, Antennas & Propagation*, Vol. 14, No. 1, 109–119, 2020.

[31] Kumar, A., A. Q. Ansari, B. K. Kanaujia, and J. Kishor, "High isolation compact four-port MIMO antenna loaded with CSRR for multiband applications," *Frequenz*, Vol. 72, No. 9-10, 415–427, 2018.

[32] Khan, M. I., S. Liu, J. Mao, A. Basit, A. Ahmed, and A. Daraz, "Electromagnetic coupling suppression of eight-ports MIMO antenna for satellite communication with neutralize block and parasitic elements," *AEU — International Journal of Electronics and Communications*, Vol. 170, 154821, 2023.